Systematic theoretical search for alloys with increased thermal stability for advanced hard coatings applications

Hans Lind, Ferenc Tasnadi and Igor Abrikosov

Original Publication:

Hans Lind, Ferenc Tasnadi and Igor Abrikosov, Systematic theoretical search for alloys with increased thermal stability for advanced hard coatings applications, 2013, New Journal of Physics, (15).
http://dx.doi.org/10.1088/1367-2630/15/9/095010

New Journal of Physics
The open access journal for physics

Systematic theoretical search for alloys with increased thermal stability for advanced hard coatings applications

H Lind[1], **F Tasnádi and I A Abrikosov**

Department of Physics, Chemistry and Biology (IFM), Linköping University, SE-58183 Linköping, Sweden
E-mail: halin@ifm.liu.se

New Journal of Physics **15** (2013) 095010 (16pp)
Received 31 May 2013
Published 17 September 2013
Online at http://www.njp.org/
doi:10.1088/1367-2630/15/9/095010

Abstract. State-of-the-art alloys for hard coating applications, such as TiAlN, are known to suffer from decreased hardness during heat treatment in excess of 900 °C due to the formation of detrimental wurtzite AlN phases. Recent research has shown that multicomponent alloying with additional transition metals (TMs) such as Cr can shift the onset of the phase transformations to higher temperatures, but a search for new alloys is generally time-consuming due to the large number of processes that influence material properties along with the large number of alloy compositions that have to be synthesized. To overcome this difficulty we carry out systematic first-principles calculations aimed at finding potential new multicomponent TM aluminum nitride alloys for advanced hard coating applications. We direct our search towards a specific property, the thermal stability of the coating. In particular, we concentrate on the thermodynamic stability of the cubic B1 TM–Al–N phase relative to the wurtzite phase, and choose the enthalpy difference between them as our search descriptor. We perform *ab initio* calculations for all TMs, considered as impurities in AlN, and identify the most promising candidates that may improve the thermal stability. We present arguments that these elements should be targeted in future in-depth studies, theoretical, as well as experimental.

[1] Author to whom any correspondence should be addressed.

Contents

1. Introduction

Hard, wear-resistant, thin films based on transition metal (TM) carbides and nitrides have been commercially available for some decades. They show a unique combination of properties, high hardness, high melting point and excellent electrical conductivity, which make them attractive in applications. Their commercial use continues to expand rapidly, stimulating profound research activity in this field [1–4]. Yet the time it takes to discover advanced materials and to prove their usefulness for the commercial market remains far too long [5]. Finding new materials is a non-trivial task, it may require looking at a large number of elements and alloys including several new and unconventional ones as well as sorting through a large selection of properties to find favorable materials. Computer simulations from first principles based on the electronic structure theory are capable of addressing these issues, e.g. through a high-throughput calculation based development approach [6].

The power of the method relies on the diversity of the possible combinations treated. On the other hand its bottlenecks are the possible incompleteness of the parameter space that the method is based on and the uncovered basic relationships in the parameter–property space, i.e. the knowledge of the parameters relevant for a property, the so-called descriptors. Without these requirements a straightforward application of the technique may be inaccurate, slow and occasionally misleading. As a matter of fact, theory is still not sufficiently developed to study such properties like hardness and ductility directly and/or accurately. Probably for this reason theoretically assisted high-throughput techniques are rarely used for the development of advanced hard materials, though there are some successful examples [7], as well as a clear need to address important technological challenges for this class of materials.

One such challenge, which is common for coating materials, is their thermal stability. It is a key parameter to ensure the efficient operation and long lifetime of a metal cutting tool insert during machining. Indeed, modern cutting tools operate at high temperatures, $\sim$1000 K and above, while the applied force of a cutting tool against the work piece, together with the minimal contact area, gives rise to stress levels of several GPa at the cutting edge [8]. The pioneering wear resistant TiN coatings were developed in the 80 s, however their deep-level oxidation at high temperature has been found to result in a significantly decreased hardness value. On the other hand, in some cases, like multicomponent AlN alloys with TMs Ti, Cr, Zr, Hf, the operation conditions are favorable, e.g. due to age hardening effects providing a material more sustainable to flank wear. For example, this was clearly demonstrated in [9] by means of *ex situ* hardness measurements of as deposited and isothermally heat treated samples of monolithic TiN

and $Ti_{0.34}Al_{0.66}N$ coatings. While the TiN coating showed an overall decrease in hardness with increased annealing temperature, Al-containing coatings, in contrast, showed the qualitatively different appearance with an almost constant hardness up to 800 °C followed by an increase in hardness, associated with the age hardening due to the spinodal decomposition [10–13]. However, a decrease of hardness was observed in $Ti_{0.34}Al_{0.66}N$ coatings at higher temperatures due to the cubic-to-wurtzite transformation of AlN indicating that the formation of wurtzite AlN phases can be highly detrimental for the coating thermal stability.

In this paper we utilize a systematic theoretical approach for exploring new hard coating materials providing good temperature resistance for improved wear resistance during metal machining. Specifically, we will address cubic to wurtzite transformation of AlN-rich precipitates in nitrides with different TM impurities. The paper is organized as follows. In section 2 we solve the task of establishing a parameter–property space for systematic (or high-throughput) theoretical processing and we define our descriptor. In section 3 we summarize theoretical methodology employed in the present study and determine an optimal level of theoretical approximations. In section 4 results of our theoretical search for new alloys will be presented and discussed. In section 5 we give a summary of this work.

2. Parameters–property relations for systematic search of alloys for hard coating applications with enhanced thermal stability

Let us first specify the parameters–property relations for systematic search of alloys for hard coating applications with enhanced thermal stability. Our starting point is that the cubic-to-wurtzite transformation of AlN-rich precipitates is highly detrimental and reduces the tool lifetime [11, 14]. Our goal, therefore, consists in suppressing, or at least postponing this transformation. Thus we will search for a TM, which being dissolved in AlN minimizes structural enthalpy difference between its cubic and wurtzite phases at equilibrium, and postpone a formation of the latter in coatings. Here our parameter space consists of elements, alloy compositions and their crystal structures, while the descriptor is given by the structural enthalpy difference at zero pressure between the cubic (B1) and wurtzite (B4) phases:

$$\Delta H_{\mathrm{B1-B4}} = H_{\mathrm{B1}}^{(\mathrm{TM-Al})\mathrm{N}} - H_{\mathrm{B4}}^{(\mathrm{TM-Al})\mathrm{N}}. \tag{1}$$

We further justify the choice of $\Delta H_{\mathrm{B1-B4}}$ as a descriptor for our systematic search. Norrby *et al* [15] observed that adding Ti to AlN stabilizes the cubic phase in comparison to the parent AlN system. Theoretical calculations carried out for bulk $Ti_{(1-x)}Al_xN$ alloys confirmed the experimental finding and explained it in terms of a decrease of the enthalpy difference $\Delta H_{\mathrm{B1-B4}}$ between the cubic and the hexagonal phases upon the introduction of Ti. A comparison of pressure–temperature phase diagrams of AlN and $Ti_{0.60}Al_{0.40}N$ alloy indicates a substantial reduction of the transition pressure for the hexagonal-to-cubic transformation in AlN doped with Ti. Similar conclusion on the stabilization effect of Ti has also been obtained in [16–18].

Another argument in setting up $\Delta H_{\mathrm{B1-B4}}$ as the descriptor for our problem can be found in [19], where a design route for the next generation of nitride alloys via a concept of multicomponent alloying is proposed. Lind *et al* [19] demonstrated that quasi-ternary (TiCrAl)N alloys decompose spinodally into (TiCr)N and (CrAl)N-rich nanometer sized regions. The spinodal decomposition resulted in age hardening, while the presence of Cr within the AlN phase delayed the formation of a detrimental wurtzite phase leading to a substantial improvement of thermal stability compared to the quasi-binary (TiAl)N or (CrAl)N alloys.

Note that theoretical studies also predicted the beneficial effect of Cr on the energetics of cubic-to-wurtzite transformation in (CrAl)N [17, 20]. Indeed, as will be demonstrated below, adding Cr impurities into AlN decreases $\Delta H_{\mathrm{B1-B4}}$.

We would like to underline, that for the purpose of this study we carry out our search on suppression of cubic to wurtzite transformation without concern to whether or not the solutions are thermodynamically stable or not. It is possible that the candidate multicomponent alloys that we find through this search are not miscible and undergo spinodal decomposition before reaching operational temperature. We present some arguments for the possibility of alloying the TM into AlN matrix, but we defer any detailed analysis of such properties for later studies. Price issue is also not a concern for our study at this stage. Moreover, we underline that we concentrate on only one mechanism for the design of new coating alloys with increased thermal stability, given by a direct suppression of cubic-to-wurtzite transformation. We recognize that there could be other possibilities for increasing the thermal stability. A formation of coherent precipitates of wurtzite phase at grain boundaries could lead to an increase of a coating thermal stability [21]. For example, there are experimental indications that this mechanism could be responsible for very high thermal stability of (TiZrAl)N coatings [22]. Thus, alloying elements, which are not found to be promising according to this study must not be ruled out from further considerations.

3. Computational details

The objective of this study is to get a quick overview of the effects of alloying AlN with different TM impurities to find potential candidates for more in-depth studies. Thus, we employ state-of-the-art, but still numerically efficient techniques. Many electron effects will be treated at the level of the generalized gradient approximation (GGA) in accordance with Perdew–Burke–Ernzerhof [23]. In principle, the importance of correlation effects in studies of TM nitrides has been pointed out, e.g. for CrN [24] and (CrAl)N [25]. Moreover, we deal with TM impurities in a semiconductor host, and a highly accurate description of this problem is a non-trivial task. Two kinds of errors, due to an underestimation of the host band gap and due to the localization error in the description of impurity states, do not necessarily cancel each other. Ivady *et al* [26] have just suggested a technique, the so-called HSE + V_w method, which combines basic ideas of the hybrid functional approach, solving the former problem and with LDA + U method solving the latter. However, HSE + V_w method is still too time consuming for the high-throughput applications, and our strategy would be to apply it in studies of the most promising alloys at the next stage. Similarly, having accurate representations of the substitutional disorder is not a high priority task at this point. This should be the subject of later studies, once we have identified the most promising alloying components that should be investigated in more detail. Since accurate representation of a disordered alloy is not a priority and since we want to model alloying with all of the transition metals we will limit ourselves to performing them with relatively small supercells.

In order to compare alloys with the B1 NaCl structure and those with the B4 wurtzite structure we model them with a $2 \times 2 \times 2$ primitive unit cell for the B1 structure and a $2 \times 2 \times 1$ primitive unit cell for the B4 structure. This gives each supercell a total of 16 atoms, 8 of which are N-atoms and the other 8 are Al/TM atoms. We substitute one Al-site for an impurity atom giving a total impurity concentration of 12.5% on the metal sublattice, see figure 1. This limited cell size means that we cannot properly represent disorder in the alloy as it becomes

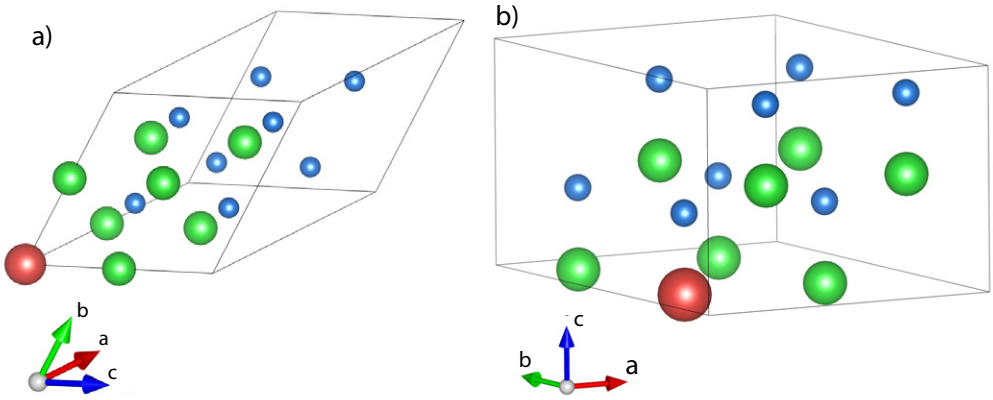

Figure 1. Schematic representations of the model structures used in the calculations. A B1 $2 \times 2 \times 2$ cell is seen in (a) and a B4 $2 \times 2 \times 1$ cell is seen in (b). Blue spheres are N-atoms, green are Al and red is the metal impurity atom.

periodic. Ionic distortions, though included in calculations, will not be fully represented due to the symmetry present, especially in the B1 structure where none of the Al-atoms and only six out of the eight N-atoms will experience local distortions. Having only one impurity atom means that disordered magnetic states cannot be fully realized either and only ferromagnetic phases can be considered using our current method for calculation as described below. Though magnetic disorder influences properties of magnetic TM nitrides [27–29], we believe that a ferromagnetic model should still be sufficient to observe the general tendencies upon alloying and allow us to choose candidates for future in-depth studies. Pure AlN is also calculated for reference, it is calculated on $1 \times 1 \times 1$ primitive unit cells for both structures, two atoms per cell for B1 and four atoms per cell for B4.

We perform density functional theory calculations using the projector augmented wave method within the Vienna *Ab initio* Simulation Package [30, 31]. We choose k-meshes of $17 \times 17 \times 17$ for the B1 structure and $12 \times 12 \times 12$ for the B4 structure, which gives an accuracy of the order of 10^{-5} eV atom^{-1} in the energy. Pure AlN is calculated using $27 \times 27 \times 27$ respectively $20 \times 20 \times 20$ k-meshes. All calculations begin with performing atomic relaxations in order to put all atoms in their equilibrium positions, these relaxations are done such that the relaxed energy is specified to within 10^{-5} eV atom^{-1}. We want both equation of state results and equilibrium states for both structures so we perform calculations on multiple volume configurations in order to generate accurate binding curves. Calculations are performed at eight different volumes and, in the case of the B4 structure, for each volume calculations are performed at seven different values of the c/a ratio. Interpolations are carried out using a simple polynomial fit to find the c/a ratio that gives the lowest energy for each volume in the B4 structure. When a volume–energy point series has been obtained a fitting curve using a modified Morse equation of state [32] method is calculated to obtain accurate equation-of-state parameters. Figure 2 shows the binding curves of AlN and TiAlN B1 and B4 structures as an example. In the image we show the binding curves with the equilibrium energies for the two structures further marked by dotted lines. Our descriptor defined above is the difference in equilibrium enthalpies at 0 K between the two structures as given by equation (1).

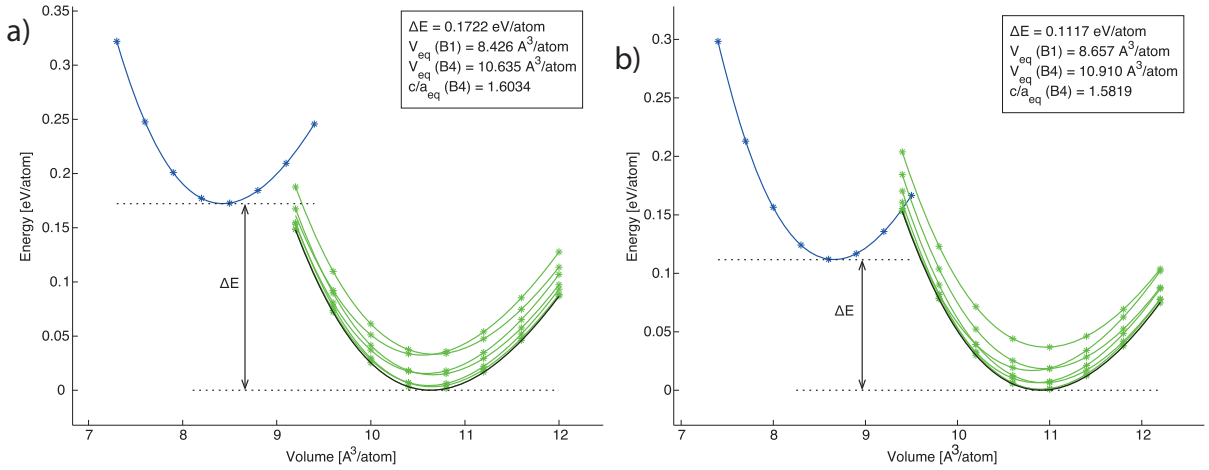

Figure 2. Binding curves of AlN (a) and TiAlN (b). Blue lines show results for B1 crystal structure and green lines correspond to systems with B4 crystal structure. The stars are the calculated data points and the lines are the Morse fitted curves. There are multiple green curves for B4 wurtzite structure, one for each c/a ratio considered by us, interpolations are done in order to find the optimal c/a ratio for any given volume and this optimized binding curve for B4 is shown by a black solid line. From this we can determine equilibrium energy, equilibrium volume and other equation of state parameters such as pressure and bulk modulus. In this example we also see how the energy difference between the two structures is reduced by the introduction of Ti into the alloy, from 0.1722 eV atom^{-1} for AlN to 0.1117 eV atom^{-1} for TiAlN.

The equilibrium enthalpy difference $\Delta H_{\mathrm{B1-B4}}$ is simply the difference in equilibrium energies, ΔE between the two structures as shown in the figure. In addition, we obtain equilibrium volumes and structural parameters for the two structures along with transition pressure as well as bulk moduli. Additional calculations are also performed at the equilibrium volume in order to obtain accurate total energies and atomic relaxations.

4. Results and discussion

The influence of TM impurity atoms on enthalpy difference $\Delta H_{\mathrm{B1-B4}}$ between the two structures is presented in figure 3 with numeric values listed in table 1. As can be clearly seen in the figure there is a general trend toward a stabilization of B1 alloys relative to systems with B4 crystal structure with TM impurities from the middle of the series, especially groups 6–9. An exception to this trend is Fe that stands out by having a much larger enthalpy difference between structures than its surrounding elements. Also Co has a notably larger enthalpy difference than its period 5 and 6 counterparts Rh and Ir. With few exceptions the general trend is that higher period TM impurities have larger enthalpy differences. The most likely explanation for this effect is the magnetism of Fe and Co as magnetic effects are known to introduce significant deviations in the trends across the TM series [33]. Also, the limitations of our structural model prevent us from treating disordered magnetism. However, a detailed understanding of this deviation, as well as qualitative explanation of the observed trends across the series goes beyond the subject matter

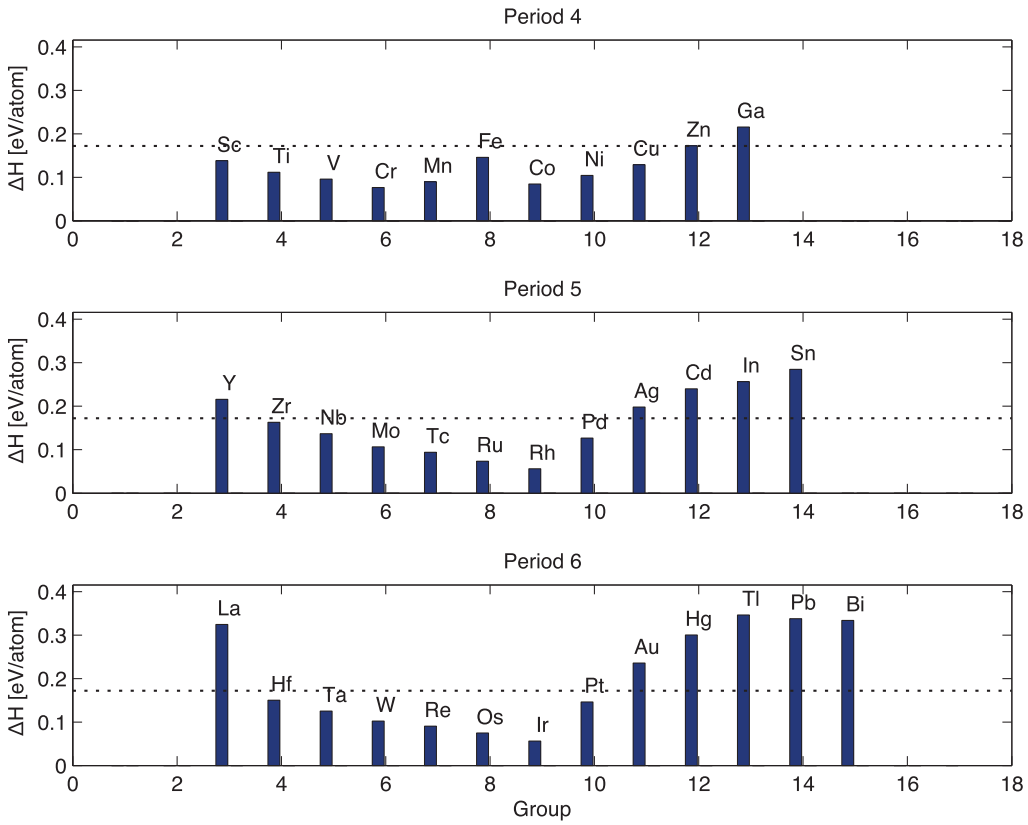

Figure 3. Variation of the enthalpy difference at zero pressure $\Delta H_{\mathrm{B1-B4}}$ equation (1), between B1 cubic and B4 wurtzite phases of doped AlN with the position of the impurity atom in the TM series. The dotted line shows pure AlN as reference. A clear trend is seen where the TMs in the middle of the periodic table, groups 6–9, iron being an exception, show a marked decrease in the enthalpy difference between the two structures.

of the present work. We therefore concentrate on our main goal, finding candidate impurities for alloying of advanced hard coatings applications.

Note that the enthalpy difference between B1 and B4 structures of AlN is 0.1722 eV atom^{-1} and is marked with a horizontal dotted line in figure 3. Known alloying elements such as Ti gives an enthalpy difference of 0.1117 eV atom^{-1} (figures 2 and 3) and Cr gives a difference of 0.0765 eV atom^{-1}. Thus, they reduce the enthalpy difference and should lead to a stabilization of the cubic phase in their respective alloys, something that has been seen in experiment. The impact of alloying AlN with Ti and Cr is well known from previous works [9–20] where TiAlN remains in a cubic B1 structure up to 60% Al on the metal sublattice. CrAlN shows even better stability of the B1 structure with a possibility of having more than 70% Al in the system. This underlines the relevance of the chosen descriptor. Moreover, our systematic calculations predict a number of candidates that result in further reduction of the enthalpy difference indicating even better thermal stability of potential multicomponent alloys. In particular Rh (0.0560 eV atom^{-1}) and Ir (0.0563 eV atom^{-1}) are such candidates but also Ru (0.0736 eV atom^{-1}) and Os (0.0746 eV atom^{-1}). Several other impurities are also noted. While in the particular regard of the enthalpy difference between the two structures, they

Table 1. Numerical values of basic thermodynamic properties obtained in this study. ΔH is the difference in equilibrium enthalpy between B1 and B4 structures by equation (1) given in eV atom^{-1}. V(B1) and V(B4) are the equilibrium volumes for B1 and B4 respectively, given in A^3 atom^{-1}. c/a(B4) is the c/a ratio in equilibrium for the B4 structure.

	ΔH	V(B1)	V(B4)	c/a(B4)
AlN	0.1722	8.4258	10.6355	1.6034
(Sc–Al)N	0.1380	8.8526	11.0879	1.5856
(Y–Al)N	0.2158	9.3584	11.5076	1.5867
(La–Al)N	0.3245	9.8860	11.8584	1.6102
(Ti–Al)N	0.1117	8.6575	10.9101	1.5819
(Zr–Al)N	0.1629	9.0964	11.2733	1.5635
(Hf–Al)N	0.1504	8.9996	11.2113	1.5741
(V–Al)N	0.0956	8.5263	10.8060	1.5915
(Nb–Al)N	0.1368	8.9107	11.0920	1.5505
(Ta–Al)N	0.1251	8.8696	11.0605	1.5543
(Cr–Al)N	0.0765	8.5266	10.7958	1.5934
(Mo–Al)N	0.1065	8.7727	10.9973	1.5612
(W–Al)N	0.1023	8.7759	10.9845	1.5646
(Mn–Al)N	0.0896	8.4024	10.6874	1.6020
(Tc–Al)N	0.0940	8.7092	10.9731	1.5792
(Re–Al)N	0.0906	8.7354	11.0135	1.6007
(Fe–Al)N	0.1459	8.3795	10.7962	1.6061
(Ru–Al)N	0.0736	8.6712	10.9645	1.5953
(Os–Al)N	0.0746	8.7113	11.0062	1.6069
(Co–Al)N	0.0847	8.3622	10.7516	1.6075
(Rh–Al)N	0.0560	8.6715	10.9828	1.5935
(Ir–Al)N	0.0563	8.7246	11.0295	1.6021
(Ni–Al)N	0.1042	8.4555	10.7426	1.6086
(Pd–Al)N	0.1269	8.8218	11.0563	1.5971
(Pt–Al)N	0.1463	8.9091	11.0920	1.5973
(Cu–Al)N	0.1289	8.5615	10.7819	1.5970
(Ag–Al)N	0.1981	8.9880	11.1896	1.6034
(Au–Al)N	0.2358	9.1027	11.2225	1.6001
(Zn–Al)N	0.1725	8.6584	10.8698	1.6260
(Cd–Al)N	0.2400	9.1154	11.2898	1.6120
(Hg–Al)N	0.3002	9.2802	11.3728	1.6117
(Ga–Al)N	0.2158	8.6162	10.8120	1.6085
(In–Al)N	0.2566	9.1417	11.2988	1.6075
(Tl–Al)N	0.3462	9.4961	11.5421	1.6168
(Sn–Al)N	0.2848	9.3317	11.4132	1.6237
(Pb–Al)N	0.3378	9.6107	11.6407	1.6225
(Bi–Al)N	0.3339	9.7449	11.7403	1.6223

seem less optimal they may still be of interest for more in-depth studies, which may reveal a combination of properties making them useful. For instance VAlN (0.0956 eV atom^{-1}), MnAlN (0.0896 eV atom^{-1}) and CoAlN (0.0847 eV atom^{-1}) alloys may be worth further consideration.

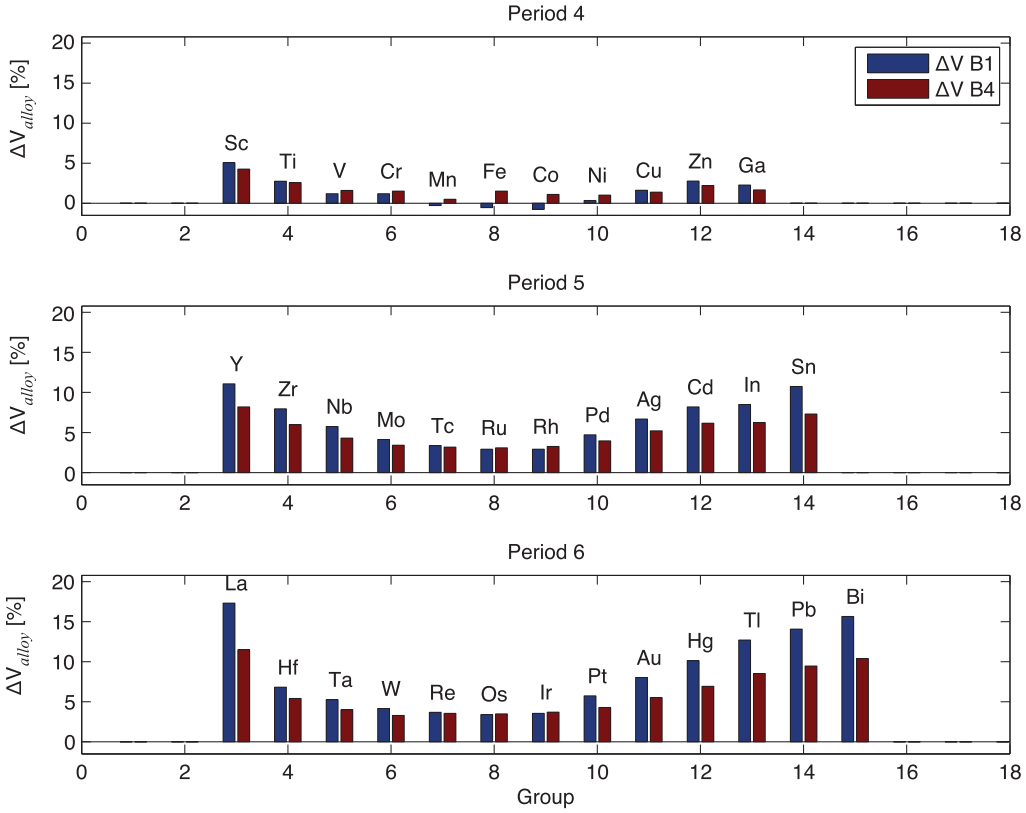

Figure 4. Change in volume ΔV_{alloy} for B1 (blue) and B4 (red) AlN doped with TM impurities relative to stoichiometric AlN.

Moreover, more advanced treatment of magnetic effects, e.g. magnetic disorder [29–31] may give somewhat different results for Fe and Co. Thus, these metals could be considered as potentially interesting alloying elements, along with other group 6–9 TM.

While the enthalpy difference $\Delta H_{\text{B1}-\text{B4}}$ is the primary descriptor for our search we also derive a number of other properties from our calculations. For instance equilibrium volumes, which are listed in table 1. Figure 4 shows the change in volume relative to pure AlN due to the introduction of the impurity

$$\Delta V_{\text{alloy}} = \left(V_{(\text{TM}-\text{Al})N} - V_{\text{AlN}}\right)/V_{\text{AlN}}. \tag{2}$$

Again we see similar trends as with the enthalpy with less increase in volume caused by the impurities of group 6–9 elements in the middle of the TM series than the ones toward the sides. For all impurities in period 4 the change in volume is quite small and only Sc in AlN with B1 crystal structure shows an increase in volume exceeding 5%. For the elements of interest mentioned above the volume increase is 2.75% for Ti in B1 AlN, and 2.58% in B4 AlN. The volume increase for Cr is even less at 1.20% for B1 alloy and 1.51% for B4 alloy. Note that in this case the volume increase is less for the B1 crystal than for the B4. We know from previous work [9–20] that TiAlN and CrAlN alloys can be synthesized in B1 crystal structure, even though, in the case of TiAlN in particular, they are metastable and decompose spinodally at higher temperature. This can be compared to ZrAlN, which in this calculation show a volume increase of 7.96% for B1 structure and 6.00% for B4 structure. ZrAlN has been shown to have

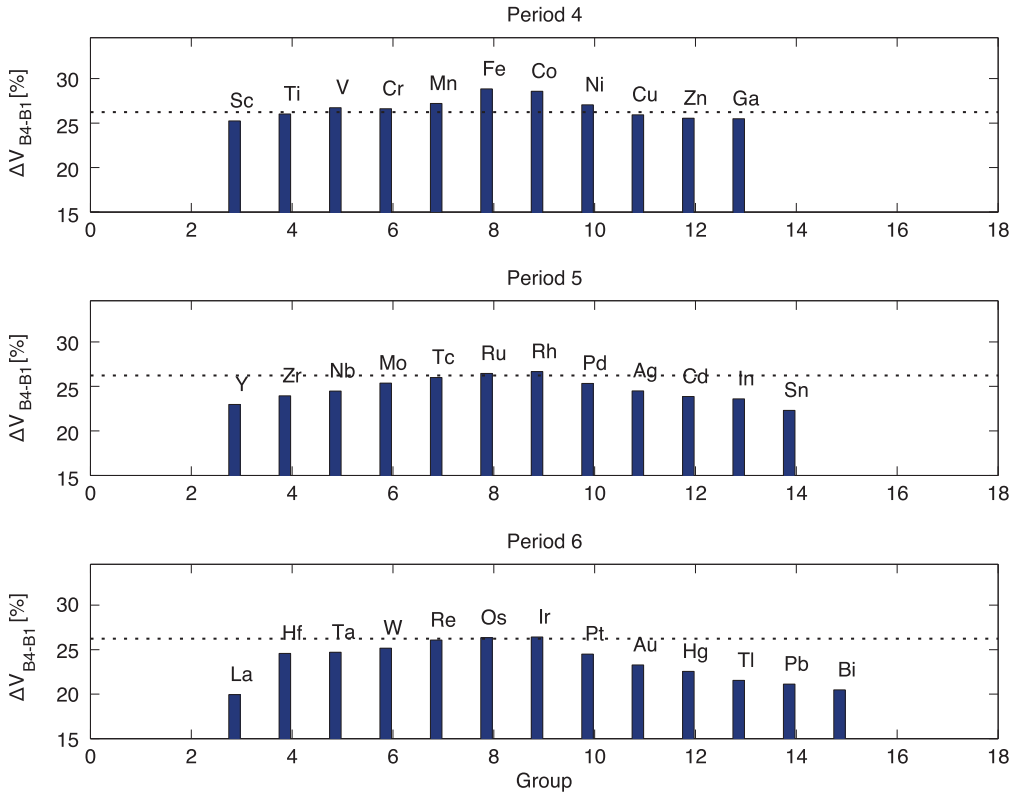

Figure 5. Relative difference in volume $\Delta V_{\mathrm{B4-B1}}$ between B1 and B4 crystal structure of AlN doped with TM impurities. AlN relative volume difference is shown as reference by the dotted line.

a very high positive formation enthalpy and has been known to be highly unstable alloy, which cannot be grown with more than 50% Al [34–35]. Mn, Fe and Co reduce the volume of the B1 structure by 0.28, 0.55 and 0.75% respectively while the volume of the B4 structure increases slightly. Rh and Ir increase the volume by 2.92 and 3.55% in B1 structure and by 3.27 and 3.70% in B4 structure. Since our primary candidates in groups 6–9 show small increases in volume due to the addition of impurities, only slightly larger than for Ti, this looks like a good indicator for a possibility to synthesize these alloys by means of thin-film growth techniques, even if they are only metastable.

Figure 5 shows the volume difference of B4 structure relative to the B1 for each impurity element with the value of AlN shown as reference as a dotted line:

$$\Delta V_{\mathrm{B4-B1}} = (V_{\mathrm{B4}} - V_{\mathrm{B1}})\,/V_{\mathrm{B1}}. \tag{3}$$

We see that group 6–10 impurity elements maintain a large volume difference between B1 and B4. In some cases, particularly for period 4 elements the difference even increases compared to AlN for which the volume of a B4 crystal is 26.2% larger than B1 in terms of volume. Apart from V, Cr, Mn, Fe, Co and Ni in period 4, Ru, Rh, Os and Ir show an increase in the volume difference between B1 and B4 compared to AlN. Rh shows a volume difference of 26.7% and Ir 26.4%. Maintaining a large volume difference between B1 and B4 structures is also important for stabilizing the B1 structure. Given that the alloy has to expand in order to realize the transition and since we know that c-AlN can be stabilized in multilayers and

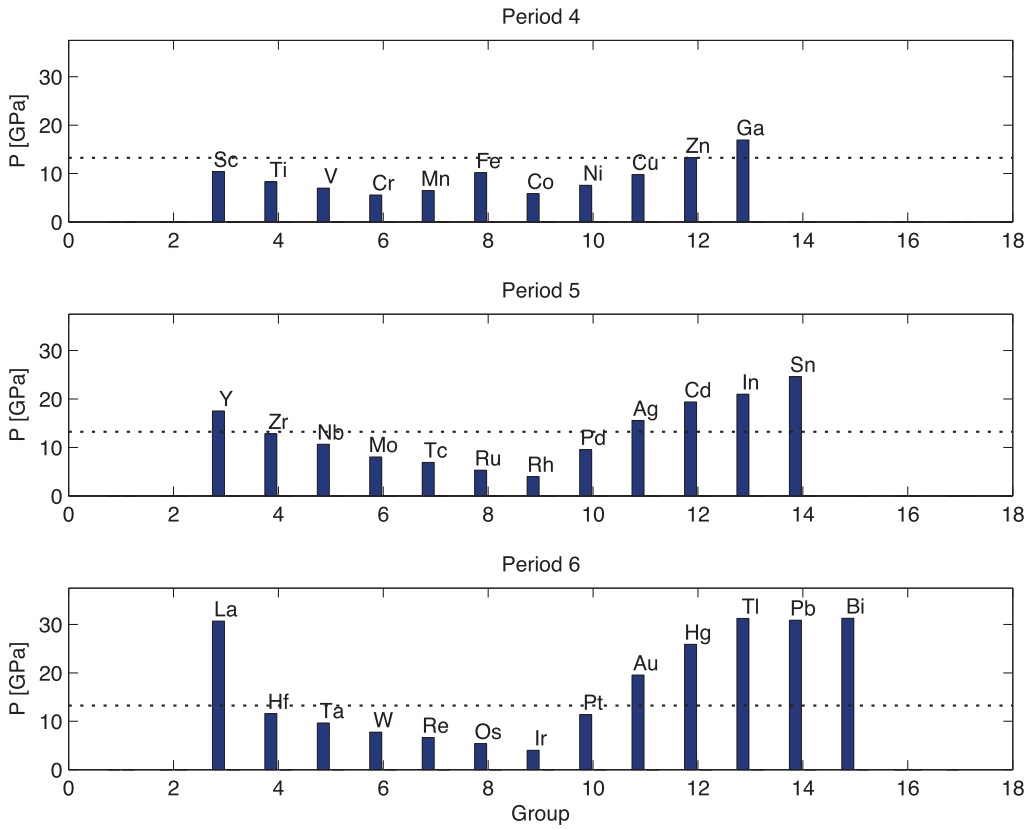

Figure 6. Zero temperature values of pressure P for B4–B1 phase transformation in AlN doped with TM impurities. The transition pressure for pure AlN is marked as a dotted line for reference.

nanostructures due to interfacial stresses we argue that a large volume difference may delay the transition when AlN-rich precipitates coexist with other phases.

Additionally, maintaining a large difference in volume will decrease the pressure for wurtzite-to-cubic phase transition, as it depends on both volume and enthalpy difference. The transition pressure from B4 to B1 at 0 K is approximately 13.23 GPa for pure AlN. Figure 6 shows the calculated transition pressure for each of the TM impurity systems with that of pure AlN marked for reference as a dotted line. We calculate the transition pressure P as the pressure at which Gibbs' free energy G is equal for both structures for the given impurity

$$G = E - TS + PV. \tag{4}$$

The transition pressure depends on both relative energies and volumes of the two structures, as well as the shape of the binding curves. Ti shows a transition pressure of 8.28 GPa, Cr brings it down to 5.55 GPa. With the exception of Fe we again see the trend of groups 6–9 giving the lowest transition pressures, particularly Ru (5.29 GPa), Os (5.37 GPa), Rh (3.97 GPa) and Ir (4.00 GPa) each of which shows a lower transition pressure than for the alloy with Cr. Numerical values for all transition pressure are listed in table 2. If the same trends we saw in pure AlN at high temperature [15] holds for the alloys, then an increase in temperature may be expected to make these alloys more stable in B1 crystal structure at high pressure. Thus, at

Table 2. Transition pressure and bulk modulus of B1 and B4 structures. P is the pressure for phase transformation from B4 to B1. Bulk modulus is in the equilibrium for B1 respectively B4 structures. Both pressure and bulk modulus are given in GPa.

	P	Bmod (B1)	Bmod (B4)
AlN	13.23	251.81	193.77
(Sc–Al)N	10.41	244.67	185.40
(Y–Al)N	17.54	227.05	175.07
(La–Al)N	30.68	210.13	164.79
(Ti–Al)N	8.28	251.43	187.76
(Zr–Al)N	12.81	241.58	181.25
(Hf–Al)N	11.57	237.49	177.19
(V–Al)N	6.96	254.71	187.68
(Nb–Al)N	10.64	248.44	180.75
(Ta–Al)N	9.65	252.87	183.34
(Cr–Al)N	5.55	253.02	190.09
(Mo–Al)N	8.04	255.62	175.53
(W–Al)N	7.75	257.93	182.53
(Mn–Al)N	6.47	257.35	194.51
(Tc–Al)N	6.91	257.44	182.82
(Re–Al)N	6.62	260.18	176.75
(Fe–Al)N	10.13	256.58	190.02
(Ru–Al)N	5.29	257.49	183.64
(Os–Al)N	5.37	261.02	182.69
(Co–Al)N	5.85	256.10	185.60
(Rh–Al)N	3.97	255.82	182.72
(Ir–Al)N	4.00	259.33	183.73
(Ni–Al)N	7.57	249.75	189.01
(Pd–Al)N	9.55	244.84	181.68
(Pt–Al)N	11.37	247.16	183.72
(Cu–Al)N	9.77	241.93	179.02
(Ag–Al)N	15.56	233.37	176.78
(Au–Al)N	19.55	235.32	179.69
(Zn–Al)N	13.29	237.55	183.18
(Cd–Al)N	19.36	227.76	176.45
(Hg–Al)N	25.88	226.14	175.81
(Ga–Al)N	16.94	250.48	192.82
(In–Al)N	20.98	239.34	183.67
(Tl–Al)N	31.25	229.49	177.76
(Sn–Al)N	24.63	225.53	174.70
(Pb–Al)N	30.86	219.70	170.78
(Bi–Al)N	31.27	217.90	168.14

elevated temperatures, some of the proposed systems may even be stable in the B1 crystal structure at ambient pressure, or at least at the operational pressures of machining tools, which can reach several GPa.

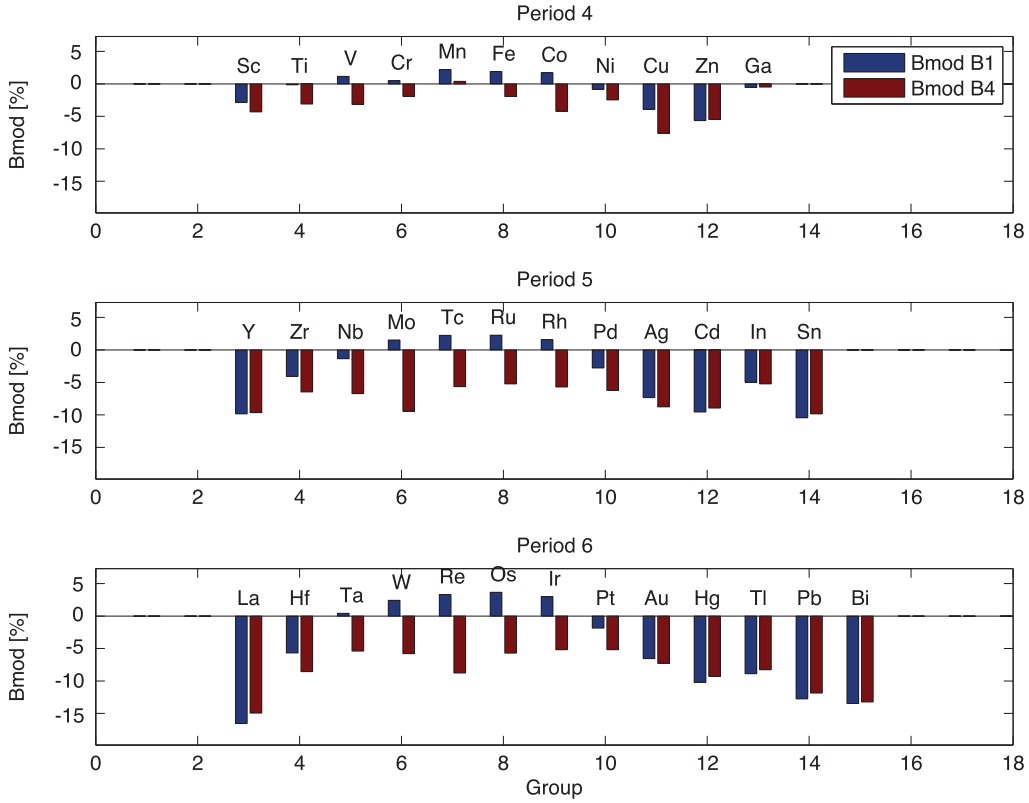

Figure 7. Change in bulk moduli of B1 (blue) and B4 (red) AlN doped with TM impurities relative to stoichiometric AlN. Calculated in the same way as ΔV_{alloy} above, but for bulk modulus instead of volume.

The bulk moduli of the alloys are given in figure 7 and table 2. The figure presents them as an increase (decrease) in per cent from the bulk modulus value of AlN (251.81 GPa for B1, 193.77 GPa for B4). Adding impurity atoms from group 6–9 increases the bulk modulus of the B1 structure making it more rigid. Os shows the biggest increase of 3.66% relative to AlN. With the only exception being Mn all other impurities softened the B4 structure although it softened less for the group 6–9 impurities than for the others.

As impurities are added to AlN local distortions of the crystal lattice occur around them due to size mismatch and electronic structure incompatibilities. As a matter of fact, their amplitudes may give some indication of the possibility to synthesize an alloy with that TM impurity as too large a lattice distortion may prevent the synthesis. Figure 8 presents the results on the local distortions of N-atoms in the B1 crystal structure for all the TM impurities. Due to the symmetry of the B1 lattice the Al-atoms will not move at all during relaxations and only six out of the eight N-atoms move, the ones at (0.25;0.25;0.25) and (0.75;0.75;0.75) are balanced between the impurities at (0;0;0), (1;0;0), (0;1;0) and (0;0;1) respectively (1;1;1), (1;1;0), (1;0;1), (0;1;1) and do not move. However the other atoms all move by equal amounts as well as equally along each three directions. The distortions presented in figure 8 are given in units of the basis vector length $\sqrt{2}a_0$ where a_0 is the fcc lattice parameter for the given alloy and are total distortions of a single atom in all three dimensions. Again we see the similar trends as before with low distortions for impurities from group 6–9. For example, Co hardly generates any distortion at all. The value

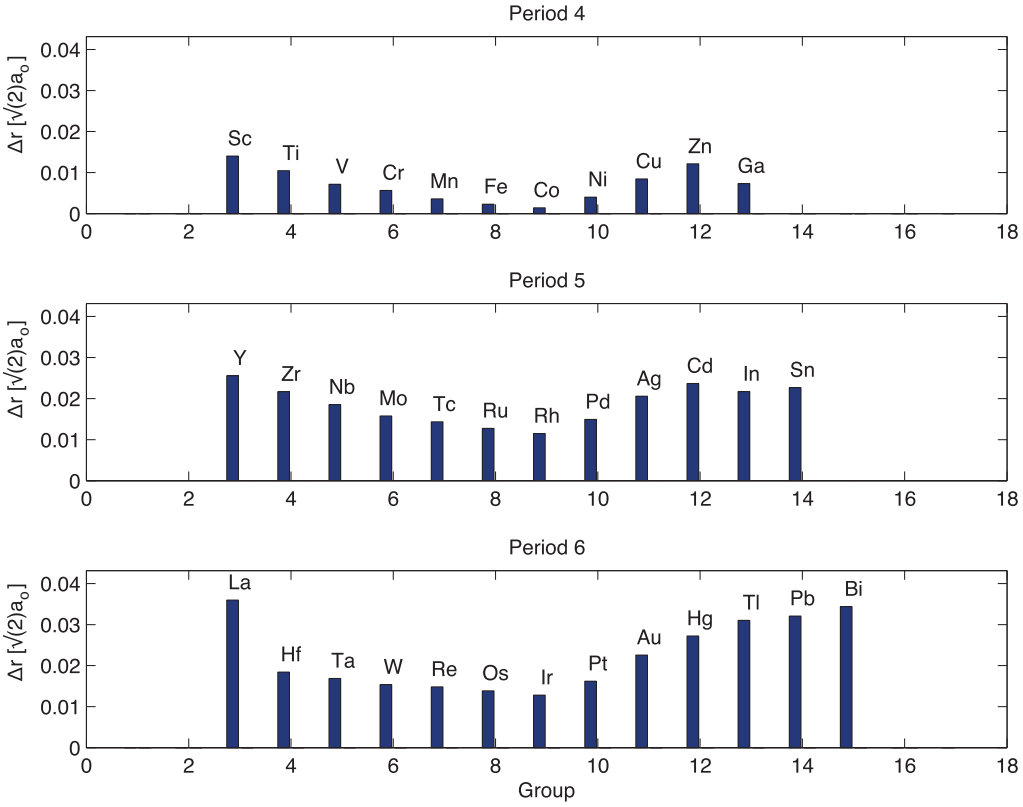

Figure 8. Deviation of N-atoms positions from the ideal crystal coordinates in B1 crystal structure, given in units of the basis vector length $\sqrt{2}a_0$ where a_0 is the fcc lattice parameter for the given alloy.

for Cr is 0.0056, respectively. Compared to Co and Cr the distortions are definitely larger for period 5 and 6 TM with Rh distorting the N-atoms by 0.0115 and Ir by 0.0128. However, in both cases they are similar to that of Ti (0.0104). As we know that Ti can be grown in solution with AlN despite positive formation energy and is capable of existing in a non-equilibrium state the possibility to synthesize the alloys look promising for our prime candidates. Zr, which is known to be difficult to grow in solution with AlN [34, 35], creates a lattice distortion of 0.0217. From this we conclude that it is unlikely that any impurity generating a distortion of 0.02 or greater can be grown in a solution with AlN. This will definitely rule out any elements in group 3, 4 or any 11 or higher within periods 5 and 6 as soluble candidates, this seems consistent with what we said above in regard to volume change of the structure as a whole.

5. Conclusions

The purpose of this paper was to carry out systematic theoretical investigation of alloying AlN with TM impurities in order to find candidate materials that may improve the thermal stability of alloys for advanced hard coatings applications, in particular with respect to a suppression of transformation from B1 cubic AlN phase into the B4 wurtzite AlN. As a descriptor in our search we use the change in alloy lattice stability measured as the enthalpy difference between the B1 and B4 crystal structures upon doping of the AlN with TM impurities. In addition, we

monitor volume change between the two structures as well as the transition pressure from B4 to B1 phase.

Our search showed that elements of group 6–9 provided the most favorable impact on these properties. The best results were seen for Ru, Os, Rh and Ir that showed significant reductions in the enthalpy difference between structures while maintaining a large volume difference, resulting in considerable lowering of the phase transition pressure. These alloys may even prove to be stable at ambient pressure at elevated temperatures but for now we have no information on their high temperature properties. While we did not undertake any formal study of solubility we see that our candidates Ru, Os, Rh and Ir have a relatively small impact on the overall volume of the alloys compared to pure AlN. We also observe that the atomic distortions around these impurities are comparable to that of Ti. This indicates that it may be possible to grow a solid solution with these alloying elements. We note that nitrides of Os and Ir have been synthesized, and the emerging field of precious metal nitrides has attracted much interest [36–38].

Of course, our prime candidates based on enthalpy difference Ru, Os, Rh and Ir are also some of the rarest and most expensive of all metals. Their period 4 counterparts Fe and Co on the other hand are far more common. Fe and Co impurities cause virtually no change in volume or atomic distortions at all, suggesting that they might be even more soluble. They do not give optimal results according to our descriptor however, deviating somewhat from observed trends across the TM series. But the deviations could be ascribed to the magnetic effects, which were treated within the simplest (ferromagnetic) model in this study. Considering larger supercells and more magnetic states, e.g. the magnetically disordered state, may therefore alter the value of the descriptor. We therefore suggest that Fe and Co are worth consideration in more detailed studies.

While the high-throughput approach has provided us with interesting candidates for synthesis of new alloys for hard coatings applications with increased thermal stability, more studies are clearly required. From the materials synthesis perspective, a proper determination of the solubility limits is highly desirable. However, this work has allowed us to locate several promising candidates on which we can concentrate future efforts and do more detailed calculations on, using larger supercells, determining solubility enthalpy and temperature based free energy through phonon calculations and disorder, as well as going beyond GGA in the treatment of many-electron effects. A detailed investigation of the electronic structure for these systems will be carried out to understand the observed trends across the TM series, which will be of high interest for physics.

We must also remember that other properties than the cubic to wurtzite transformation influence thermal stability, as was discussed in section 2. Thus, materials ruled out as potential candidates in this study should not be eliminated from consideration in other projects.

Acknowledgments

We gratefully acknowledge highly beneficial discussions with Professor M Odén and Professor M P Johansson. This work was supported by the Swedish Foundation for Strategic Research (SSF) through the project Designed multicomponent coatings, MultiFilms, and SRL grant no. 10-0026 as well as by the Swedish Research Council grant no. 621-2011-4426. Calculations were carried out at the Swedish National Infrastructure for Computing (SNIC).

References

[1] Hultman L, Engström C and Odén M 2000 *Surf. Coat. Technol.* **133–134** 227–33
[2] Mayrhofer P H, Hörling A, Karlsson L, Sjölén J, Mitterer C and Hultman L 2003 *Appl. Phys. Lett.* **83** 2049
[3] Mayrhofer P H, Music D and Schneider J M 2006 *Appl. Phys. Lett.* **88** 071922
[4] Mayrhofer P H, Music D and Schneider J M 2006 *J. Appl. Phys.* **100** 094906
[5] The Materials Genome Initiative for Global Competitiveness 2011 www.whitehouse.gov/sites/default/files/microsites/ostp/materials_genome_initiative-final.pdf
[6] Curtarolo S, Hart G L W, Nardelli M B, Mingo N, Sanvito S and Levy O 2013 *Nature Mater.* **12** 191
[7] Bolvardi H, Emmerlich J, Baben M T, Music D, von Appen J, Dronskowski R and Schneider J M 2013 *J. Phys.: Condens. Matter* **25** 045501
[8] M'Saoubi R and Ruppi S 2009 *CIRP Ann.* **58** 57
[9] Knutsson A, Johansson M P, Karlsson L and Odén M 2010 *J. Appl. Phys.* **108** 044312
[10] Hörling A, Hultman L, Odén M, Sjölén J and Karlsson L 2002 *J. Vac. Sci. Technol.* A **20** 1815–23
[11] Hörling A, Hultman L, Odén M, Sjölén J and Karlsson L 2005 *Surf. Coat. Technol.* **191** 384–92
[12] Rachbauer R, Massl S, Stergar E, Holec D, Kiener D, Keckes J, Patscheider J, Stiefel M, Leitner H and Mayrhofer P H 2011 *J. Appl. Phys.* **110** 023515
[13] Alling B, Ruban A V, Karimi A, Peil O E, Simak S I, Hultman L and Abrikosov I A 2007 *Phys. Rev.* B **75** 045123
[14] Knutsson A, Johansson M P, Karlsson L and Odén M 2011 *Surf. Coat. Technol.* **205** 4005–10
[15] Norrby N, Lind H, Parakhonskiy G, Johansson M P, Tasnádi F, Dubrovinsky L S, Dubrovinskaia N, Abrikosov I A and Odén M 2013 *J. Appl. Phys.* **113** 053515
[16] Alling B, Odén M, Hultman L and Abrikosov I A 2009 *Appl. Phys. Lett.* **95** 181906
[17] Holec D, Rovere F, Mayrhofer P H and Barna P B 2010 *Scr. Mater.* **62** 349–52
[18] Mayrhofer P H, Rachbauer R and Holec D 2010 *Scr. Mater.* **63** 807–10
[19] Lind H, Forsén R, Alling B, Ghafoor N, Tasnádi F, Johansson M P, Abrikosov I A and Odén M 2011 *Appl. Phys. Lett.* **99** 091903
[20] Mayrhofer P H, Music D, Reeswinkel Th, Fuß H G and Schneider J M 2008 *Acta Mater.* **56** 2469–75
[21] Höglund C, Alling B, Birch J, Manfred B, Persson P O Å, Baehtz C, Czigány Z, Jensen J and Hultman L 2010 *Phys. Rev.* B **81** 223101
[22] Rogström L, Ghafoor N, Ahlgren M and Odén M 2012 *Thin Solid Films* **520** 6451–4
[23] Perdew J P, Burke K and Ernzerhof M 1996 *Phys. Rev. Lett.* **77** 3865
[24] Alling B, Marten T and Abrikosov I A 2010 *Nature Mater.* **9** 283
[25] Alling B, Hultberg L, Hultman L and Abrikosov I A 2013 *Appl. Phys. Lett.* **102** 031910
[26] Ivady V, Abrikosov I A, Janzen E and Gali A 2013 *Phys. Rev.* B **87** 205201
[27] Alling B, Marten T, Karimi A and Abrikosov I A 2007 *J. Appl. Phys.* **102** 044314
[28] Alling B, Marten T and Abrikosov I A 2010 *Phys. Rev.* B **82** 184430
[29] Steneteg P, Alling B and Abrikosov I A 2012 *Phys. Rev.* B **85** 144404
[30] Kresse G and Hafner J 1994 *Phys. Rev.* B **49** 14251
[31] Kresse G and Furthmüller J 1996 *Phys. Rev.* B **54** 11169
[32] Moruzzi V L and Janak J F 1988 *Phys. Rev.* B **37** 790
[33] Pettifor D G 1995 *Bonding and Structure of Molecules and Solids* (Oxford: Clarendon)
[34] Rogström L, Ahlgren M, Almer J, Hultman L and Odén M 2012 *J. Mater. Res.* **27** 1716
[35] Holec D, Zhou L, Rachbauer R and Mayrhofer P H 2013 *J. Appl. Phys.* **113** 113510
[36] Crowhurst J C, Goncharov A F, Sadigh B, Evans C L, Morrall P G, Ferreira J L and Nelson A J 2006 *Science* **311** 1275
[37] Yu R, Zhan Q and De Jonghe L C 2007 *Angew. Chem. Int. Edn Engl.* **46** 1136–40
[38] Åberg D, Sadigh B, Crowhurst J and Goncharov A F 2007 *Phys. Rev. Lett.* **100** 095501